



# Effect of structure of high entropy CrFeCoNiCu alloys produced by EB PVD on their strength and dissipative properties



A.I. Ustinov<sup>a</sup>, S.A. Demchenkov<sup>a,\*</sup>, T.V. Melnychenko<sup>a</sup>, V.S. Skorodzievskii<sup>b</sup>, S.S. Polishchuk<sup>b</sup>

<sup>a</sup> E.O. Paton Electric Welding Institute, 11 Kazymyr Malevych Str., Kyiv 03150, Ukraine

<sup>b</sup> G.V. Kurdyumov Institute for Metal Physics, 36 Vernadsky Str., Kyiv 03142, Ukraine

## ARTICLE INFO

### Article history:

Received 12 May 2021

Received in revised form 19 July 2021

Accepted 29 July 2021

Available online 31 July 2021

### Keywords:

High-entropy alloys

Physical vapor deposition

Vacuum condensate

Hardness

Plasticity

Damping capacity

## ABSTRACT

Thin (up to 100  $\mu\text{m}$ ) foils and coatings of high-entropy CrFeCoNiCu<sub>x</sub> ( $x = 0...3.0$ ) alloys (HEAs) were produced at different temperatures in the 525...1275 K range by electron-beam evaporation of ingots. It is shown that CrFeCoNiCu<sub>x</sub> (where  $x > 0.3$ ) condensates deposited at a temperature above 925 K have a dual-phase structure consisting of two FCC phases, while those deposited at a temperature below this value exhibit a single-FCC structure. It is also found that annealing of the deposited single-phase CrFeCoNiCu<sub>x</sub> ( $x = 0.3...3.0$ ) condensates at temperatures above 925 K results in the transition into a dual-FCC phase state. Yet, condensates with the copper content  $x < 0.3$  remain stable at heating up to high temperatures (up to 1300 K). The transition from single-phase condensates into dual-phase condensates occurs through the formation of the metastable Cr-enriched phase. The effect of the condensate structure on their mechanical and dissipative properties is considered. The single-phase condensates exhibit increased microhardness, as compared to the cast alloy. The microhardness of the two-phase condensates is lower than in single-phase ones but still higher than in the cast ingot. HEA-based vacuum condensates in both single-phase and two-phase states show high values of damping capacity, which are comparable with those of highly damping materials, such as AZ31B-F magnesium alloys.

© 2021 Elsevier B.V. All rights reserved.

## 1. Introduction

Complex solid solutions, usually containing at least five elements with 5–35 at% concentration of each of them, and often referred to as high-entropic alloys (HEA) in publications [1], are characterized by high strength and ductility [2,3], thermal stability [4], high wear resistance and corrosion resistance [5], as well as hydrophobicity [6] good weldability [7] and promising irradiation resistant behavior [8]. It is worth also noting that some HEAs exhibit interesting damping properties [9], which is particularly important for preventing the excitation of resonant vibrations in thin-walled thermal protection tile structures [10], operating under conditions of vibration loadings. The unusual combination of properties in such multicomponent alloys also promotes greater interest in possible applications of HEAs in the form of coatings, thin films and foil. To date, there is a sufficiently large number of works devoted to studying the structure and properties of HEA films and coatings produced by the methods of magnetron sputtering [6,11–15], cathodic-vacuum-arc-vapor

deposition [16], thermal spraying [17,18], and electron-beam physical vapor deposition (EB PVD) [19].

It is also known that properties of materials are determined by their chemical and phase compositions, as well as by the features of their microstructure. For example, in case of HEAs of the Cr-Fe-Co-Ni-Cu system the high enthalpy of mixing of copper and other elements in this alloy results in copper segregation in interdendritic areas during melt crystallization that later on leads to the formation of nano-sized precipitates of the copper-based hard phase, and it can affect both the strength and ductility of such alloys [20,21]. Many authors note that multicomponent systems, stabilization of which in solid solution condition is related to configurational entropy, can undergo phase and structural changes under certain temperature conditions, which are due to the initial solid solution decomposition and/or formation of intermetallic compounds [6,22–25]. Moreover, analysis of published data shows that the method of producing HEA can also influence their phase composition, and microstructure. So, for instance, it turned out that in the case of a well-studied HEA of Cr-Fe-Co-Ni-Cu system at its production by metallurgical methods, in one case just two FCC phases were observed, both in the initial condition, and after high-temperature treatment [26], whereas in another case inclusions of a third chromium-rich FCC phase were

\* Corresponding author.

E-mail address: [s\\_demchenkov@ukr.net](mailto:s_demchenkov@ukr.net) (S.A. Demchenkov).

detected, in addition to the two FCC phases. It remained stable even after long-term annealing at the temperature of 1623 K [23]. At the same time, at heating of CrFeCoNiCu HEA, produced by mechanical alloying, formation of metastable  $\sigma$  and ordered BCC phases is noted [24], and in the case of thin films, produced by magnetron sputtering, the authors [25] note formation of a metastable BCC phase in a diffusionless mode at the temperature of the order of 673 K.

From this view point, an important task at assessment of potential practical application of HEA is establishing the regularities of phase and structural transformation in such materials that will allow prediction of their behaviour and properties.

We showed earlier [27] that the method of EB PVD of HEA ingots based on the Cr-Fe-Co-Ni-Cu system enables producing thin foils and coatings that seem to be promising for practical application of these alloys as materials for thin-walled structures or functional coatings. At the same time, the effect of the structure of the CrFeCoNiCu HEAs produced from the vapor phase on their mechanical properties has been not yet conducted. In this connection, the effect of structural features of HEA vacuum condensates in an as-deposited state and after heat-treatment on their strength and damping properties was studied in this work.

## 2. Material and methods

Thin foils of the Cr-Fe-Co-Ni-Cu system were produced by electron beam evaporation of the CrFeCoNiCu ingot, followed by vapor deposition on stainless steel (AISI 302) substrates heated to the specified temperature. Initial ingots of CrFeCoNiCu<sub>x</sub> (where x = 0...3) alloys were prepared using an induction furnace. To produce foil, a thin layer of CaF<sub>2</sub> was preliminarily deposited on the substrate, and then HEA deposition was carried out. CrFeCoNiCu foils of 40–100  $\mu\text{m}$  thickness were deposited at a rate of about 100 nm / s at substrate temperatures in the range of 525...1275 K. During subsequent cooling of the substrate to room temperature, the vacuum condensate layer separates easily from the substrate in the form of thin foil, due to the difference in CTE of the substrate and condensate materials.

Coatings based on these alloys were deposited on substrates made from a Ti-6Al-4V alloy sheet. A bond coating of copper with a thickness of 5  $\mu\text{m}$  was pre-deposited on the substrate to enhance the bond of the coating with the substrate.

The chemical composition of the condensate produced under various conditions was investigated by X-ray fluorescence analysis in the X'Unique-II system. Element distribution along the thickness of the condensate was determined by the method of local microanalysis in the scanning electron microscope (SEM) CamScan4, fitted with energy-dispersive analysis system EDX INCA 200.

X-ray diffractometer DRON-4M (Co-K $\alpha$  radiation) was used to conduct phase and X-ray diffraction analysis. To perform in-situ diffraction analysis during heating and annealing, a vacuum chamber with a heater was placed on the X-ray diffractometer, and the slot detector was replaced by a curved position-sensitive detector that allowed obtaining diffraction patterns in the range of angles of up to 40 degrees at continuous heating (20 K / min) of the sample or the specified temperature after fixed time intervals.

The mechanical properties of CrFeCoNiCu bulk alloy and foils at static loading were studied by the indentation method. For this purpose, the foils were pressed into resin and their transverse sections were prepared. Identification was performed by the Berkovich diamond pyramid ( $\alpha = 65^\circ$ ) in Micron-gamma unit [28] at the load of 0.4 N and loading rate of 0.04 N / s in the automatic mode. Recording of the experimental points in the form of a diagram with the coordinates of "P (load) - h (penetration depth of the indenter)" of the loading-unloading process was performed automatically. The following characteristics were determined by the obtained data: microhardness ( $H_\mu$ ), Young's modulus (E) and coefficient of plasticity

( $\delta_{pl}$ ), calculated by the following formula [29]:  $\delta_{pl} = \frac{W_p}{W_t} = 1 - \frac{W_e}{W_t}$ , where  $W_p$ ,  $W_e$ , and  $W_t$  are the work consumed for plastic, elastic and total deformation, respectively when the indenter is applied. The  $W_e/W_t$  ratio was determined by the ratio of the areas under the unloading and loading curves.

Dissipative properties of the HEAs CrFeCoNiCu were studied using the special equipment described in the works [30,31]. The samples were cantilever-fixed 1.8 mm thick substrates with 70...100  $\mu\text{m}$  thick coatings deposited on them.

The damping capacity (DC) of the samples with coatings was characterized by the amplitude dependencies of the logarithmic decrement (LD)  $\delta_s(\varepsilon_{av})$  where  $\varepsilon_{av}$  is the averaged strain amplitude along the surface area of the coated substrate. These data were obtained for damped bending vibrations of the samples with a frequency of 110...120 Hz, at temperatures of 295...720 K, and strain amplitudes of the coating  $\langle \varepsilon \rangle = 5 \cdot 10^{-5} \dots 8 \cdot 10^{-4}$ . Besides, the DC characteristics of the coating material at temperatures of 295...670 K were calculated according to the procedure [32]. These data are presented in the form of amplitude dependences of the loss factor  $\eta(\varepsilon)$  which is related to the logarithmic decrement of free oscillations by the relation [33]:  $\eta(\varepsilon) = \frac{\delta(\varepsilon)}{\pi}$ .

## 3. Results and discussion

### 3.1. Effect of deposition temperature on the structure of CrFeCoNiCu vacuum condensates

To study the effect of the temperature of vapor phase deposition on the structure of vacuum condensates of CrFeCoNiCu HEAs, thin foils were produced at specified substrate temperatures in the range of 523...1275 K. Fig. 1a shows the general view of the foil produced by electron beam evaporation of the CrFeCoNiCu ingot and vapor phase condensation on the substrate heated to the temperature of 1025 K. By the results of microstructural investigations by SEM method, one can see that CrFeCoNiCu condensate does not contain visible pores, cracks, or growth defects. The homogeneity of component distribution by foil thickness (Fig. 1b and Table 1) is indicative of the fact that vapor phase deposition was performed in the stationary evaporation mode.

X-ray diffraction analysis of the initial CrFeCoNiCu ingot of equiatomic composition and condensates deposited at temperatures above 1025 K revealed that X-ray diffraction (XRD) patterns are similar (Fig. 2). One can see that in both cases the XRD patterns contain two FCC phases with close lattice parameters, which is typical for HEAs of this system. The foils, deposited at temperatures below 925 K have one FCC phase. At evaporation of CrFeCoNiCu<sub>x</sub> ingots with the copper concentration in the range of x = 0...0.3 the foil structure remains single-phase, irrespective of deposition temperature.

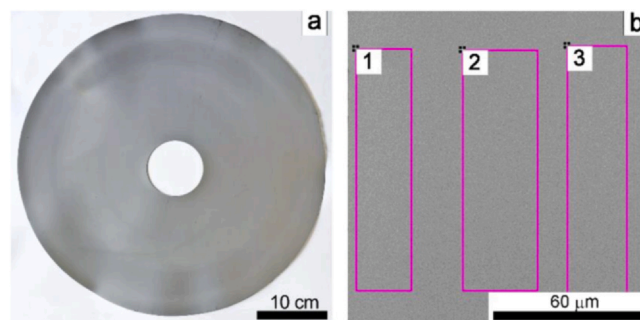
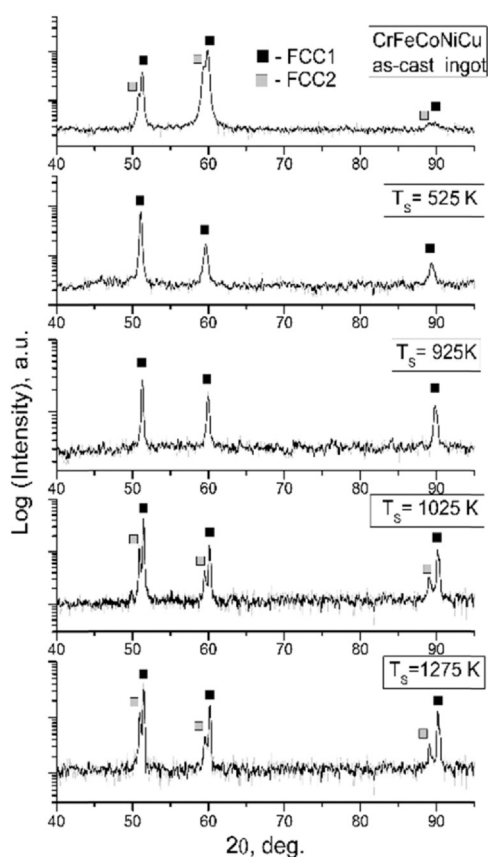


Fig. 1. General view of the CrFeCoNiCu foil produced by EB-PVD (a) and SEM image of its cross-sectional microstructure (b).

**Table 1**

Chemical composition of different areas of the CrFeCoNiCu foil cross-sectional microstructure (Fig. 1b).

Area number	Chemical composition, at%				
	Cr	Fe	Co	Ni	Cu
#1	19.6	20.5	20.5	20.1	19.3
#2	20.6	19.5	20.2	20.0	19.7
#3	21.5	18.9	19.4	18.7	21.5



**Fig. 2.** XRD patterns of CrFeCoNiCu ingot and foils deposited at different substrate temperatures.

The generalized diagram of phase composition of vacuum condensate, depending on the substrate temperature and chemical composition of the evaporation ingot of CrFeCoNiCu<sub>x</sub> alloy is shown in Fig. 3. One can see that vacuum condensates of CrFeCoNiCu<sub>x</sub> HEA can be divided into two groups, depending on chemical composition: HEA with low copper content ( $x < 0.3$ ), where phase composition does not change at the increase of deposition temperature, and HEA with higher copper content ( $x > 0.3$ ), where phase composition depends on condensation temperature. A single-phase structure of the condensate forms at temperatures below a certain critical value (about 925 K), and a two-phase structure appears at temperatures above the specified one.

Values of the average crystallite size (coherent-scattering regions) in CrFeCoNiCu foils deposited at different substrate temperatures were estimated by modified Williamson-Hall method. It is seen from Fig. 4 that the crystallites size of foils deposited at substrate temperature below 850 K is smaller than 100 nm. It is also clear that the crystallite size in the foils increases with deposition temperature, which can be related to the increase in both surface diffusion of atoms on substrate and grain growth rate.

Typical microstructures of the cross-section of foils deposited at the substrate temperature of 775 and 1025 K are shown in Fig. 5. The

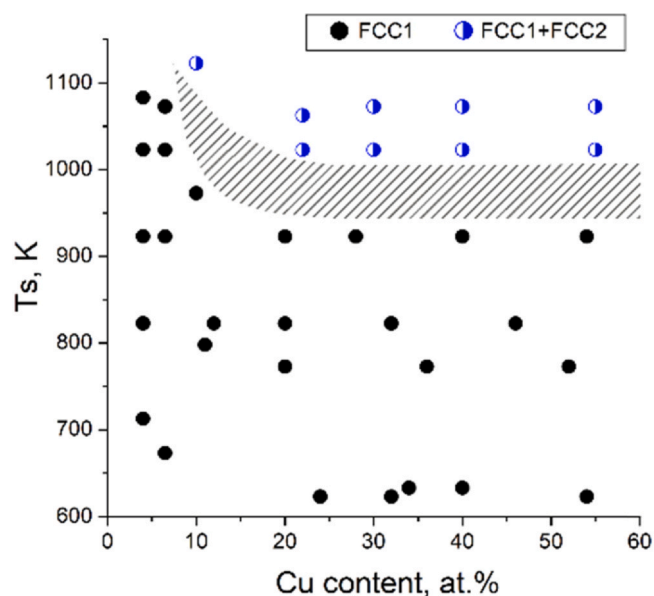


**Fig. 3.** The generalized diagram of phase composition of CrFeCoNiCu<sub>x</sub> vacuum condensate depending on the substrate temperature and Cu content.

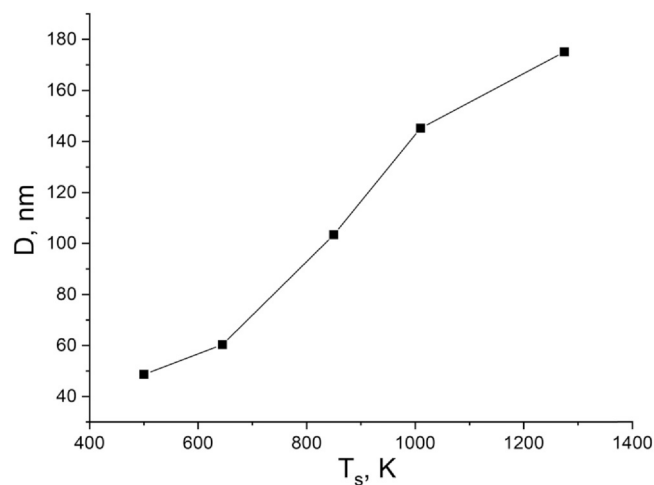


**Fig. 4.** The dependence of average coherent-scattering regions in foils on deposition temperature.

foil produced at the substrate temperature of 775 K, has a single-phase structure with grains elongated in the vapor flow direction with 0.2...0.7 μm cross-

sectional dimension (Fig. 5a). At the increase of vapor flow deposition temperature up to 1025 K, the transverse dimension of foil grains increase up to 1.2...1.5 μm and they are characterized by banded substructure, consisting of fibers with different phase contrast (Fig. 5b).

A two-phase structure of CrFeCoNiCu HEA is observed also in cast ingots (Fig. 6). Chemical analysis of grains with different contrast in the ingots showed that grains with light contrast consist predominantly of copper with Cr, Fe, Co, and Ni impurities, while grains with dark contrast are characterized by the equiatomic ratio of Cr, Fe, Co, Ni, and lower copper content. (Table 2).

It is seen also from Fig. 2 that the diffraction patterns of the ingot and the foil deposited at 1025 K are similar and are characterized by split peaks from FCC lattices with different parameters: doublet peaks from the side of smaller diffraction angles are located closer to pure copper peaks (further on FCC2-phase), while the position of doublet peaks, located from the side of great diffraction angles, is

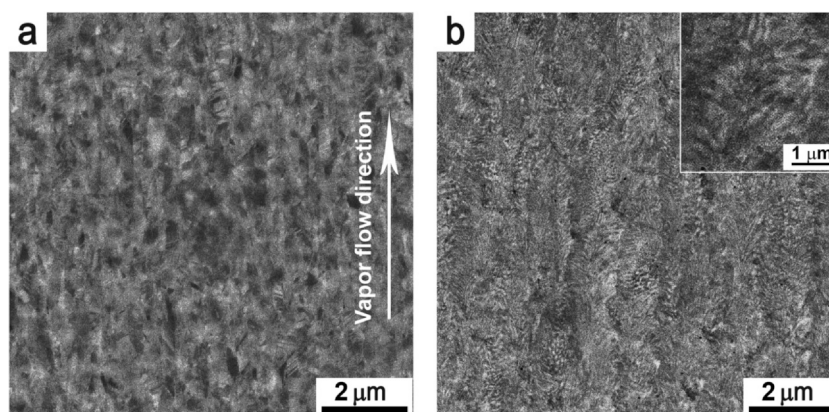


Fig. 5. SEM images of cross-sections of CrFeCoNiCu foil (BEI), produced at substrate temperature 775 K (a) and 1025 K (b).

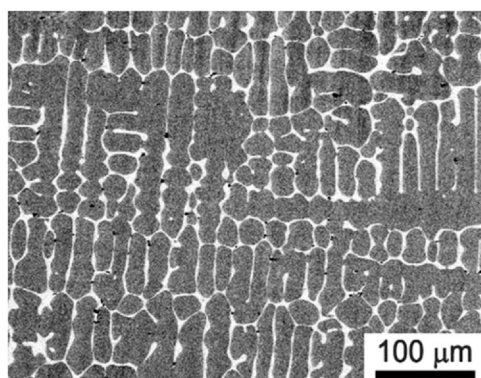


Fig. 6. SEM image of the CrFeCoNiCu ingot.

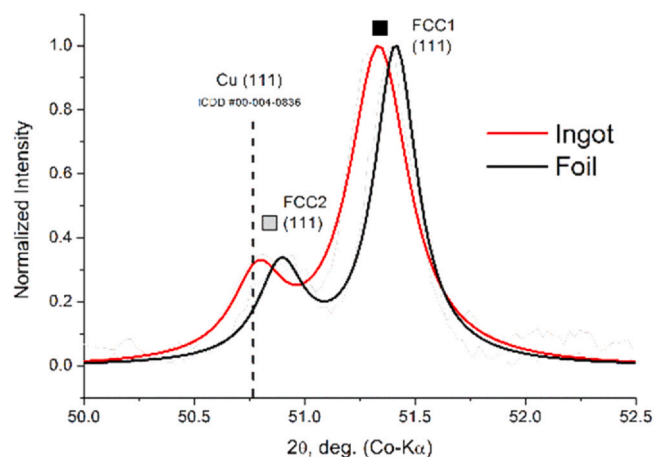


Fig. 7. Profiles of diffraction (111) peaks of FCC1 and FCC2 phases for the as-cast CrFeCoNiCu ingot and foil deposited at substrate temperatures of 1025 K.

Table 2

Chemical composition of different areas of the CrFeCoNiCu alloy microstructure (Fig. 6).

	Chemical composition, at%				
	Cr	Fe	Co	Ni	Cu
Light areas	1.9	2.9	2.6	8.3	84.3
Dark-areas	22.6	21.7	22.1	22.3	11.3

close to that of peaks of single-phase FCC structure with element ratio inherent to the ingot (FCC1).

Based on this, it was assumed that the light areas in the images of foil microstructure are also enriched in copper, and the dark ones are enriched in lighter atoms of Cr, Fe, Co, and Ni. On the other hand, unlike the ingot structure, which forms during melt solidification, the decomposition of the condensate structure is controlled by the processes running both at vapor condensation and foil annealing directly during its deposition. Therefore, the degree of HEA decomposition into two solid solutions for the ingot and vacuum condensate can differ.

Comparison of the profiles of doublets from the ingot and the foil produced at the temperature of 1025 K, shows (Fig. 7) that the positions of their components somewhat differ. The difference of FCC2-phase lattice parameters can be indicative of the fact that their chemical composition is also somewhat different: the FCC2-phase in the ingot contains a higher concentration of copper than that in the condensate.

From the comparison of the characteristic features of the microstructure of the ingot and vacuum condensate (Fig. 5b and Fig. 6), one can see that in both cases the morphologies of areas with the light or dark contrast differ qualitatively. In the case of the ingot,

coarse grains of FCC1-phase (dark contrast) are observed, with FCC2-phase precipitates (light regions) located along their boundaries.

The microstructure of vacuum condensate is characterized by grains, the substructure of which consists of alternating dark and light regions, forming a wavy grain contrast. Therefore, FCC2-phase forms individual grains in the ingot, whereas in the case of vacuum condensates, FCC2-phase is an element of grain substructure, alternating with similar elements of the FCC1-phase.

Such a difference in the morphology of structural components of the foil and the ingot leads to the assumption that the alloy decomposition into two structural components is realized by different mechanisms. In the case of the ingot, alloy decomposition occurs during its crystallization, in the temperature region of the solid-liquid state, when nucleation of grains of FCC1-phase having a higher melting temperature, initiates copper outgassing to their boundaries. The liquid phase, enriched in copper, is crystallized at a lower temperature, which is exactly what leads to the observed microstructure – FCC1-phase grains are fringed by grains of copper-based FCC2-phase.

A strip-colored contrast of vacuum condensate grains can form as a result of both solid-phase reaction of decomposition of the Cu-based supersaturated solid solution of CrFeCoNiCu alloy, for instance as a result of spinodal decomposition mechanism, and during crystallization of its vapor phase, when simultaneous growth of the two phases is realized due to high diffusion rate of atoms on the condensation surface, similar to the formation of a eutectic structure from the melt. The possibility of realization of the spinodal mechanism of decomposition in HEAs produced during high-speed

hardening was reported in work [34]. It is clear, however, that irrespective of the mechanism of vacuum condensate decomposition into components, which occurs during its formation from the vapor phase, the degree of FCC2-phase depletion in Cr, Fe, Co, and Ni atoms can be smaller than under the conditions of melt crystallization. This is exactly what explains the difference between the FCC2-phase lattice parameters in the ingot and the vacuum condensate (Fig. 7).

Lower diffusion mobility of atoms in the solid phase, probably, also causes the formation of single-phase FCC structure of the vacuum condensate (further on FCC1-phase) at vapor phase deposition at temperatures below 925 K, the chemical composition of which corresponds to the chemical composition of the ingot. In this case, a single-phase structure in vacuum condensates of CrFeCoNiCu<sub>x</sub> HEA with  $x > 0.3$  can decompose during annealing at temperatures ensuring high diffusion mobility of atoms in the solid solution. Structural changes in single-phase foils based on CrFeCoNiCu<sub>x</sub> HEAs with  $x > 0.3$  during their annealing at elevated temperatures, were studied to test this assumption.

### 3.2. Impact of annealing on the microstructure of CrFeCoNiCu condensates with single-phase structure

The method of high-temperature in-situ X-ray diffractometry was used to determine (Fig. 8) that at the heating of CrFeCoNiCu foil deposited at the substrate temperature of 775 K, up to the temperature of 1025 K a significant lowering of the intensity of diffraction peak (111) of the initial FCC1-phase takes place, and it becomes wider. Further soaking at the temperature of 1025 K, leads to splitting of this diffraction peak, and after annealing for approximately 15 min, two diffraction peaks become visible in the studied region of the diffraction pattern.

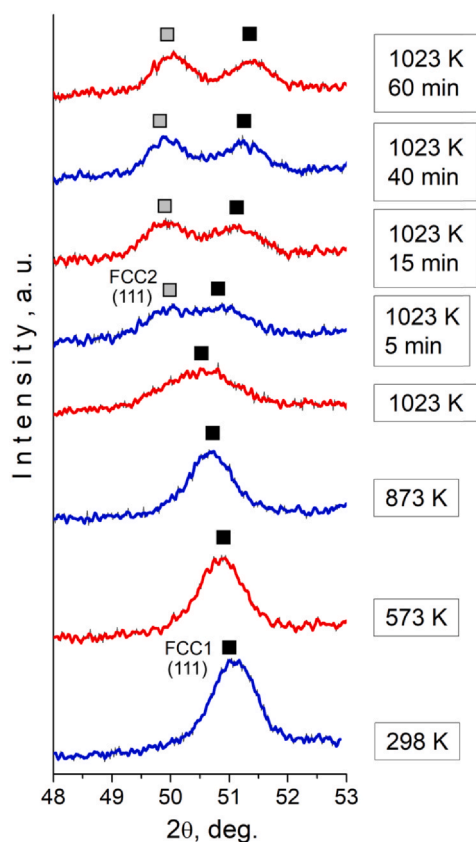


Fig. 8. In-situ XRD patterns were obtained during heating of CrFeCoNiCu foil deposited at the substrate temperature of 775 K.

It should be noted that with longer soaking time an increase of the interval between the formed peaks is observed that may be indicative of the change in crystalline lattice parameters of the formed FCC solid solutions, as a result of element redistribution between them.

It was assumed that such heat treatment results in the transformation of the single-phase state into the two-phase state, consisting of two FCC-phases (FCC1 + FCC2) in the foil, similar to the one observed in foils deposited at substrate temperature above 925 K (Fig. 2).

Analysis of the annealed foil microstructure by SEM (Fig. 9a) showed that three regions differing in their contrast can be singled out in the foil structure: dark-grey, light-colored, and light-grey.

One can see from the distribution of element concentration along the line passing through regions with different contrast (Fig. 9b) that the dark-grey regions are enriched in chromium, light-colored regions – in copper, while light-grey regions are characterized by the ratio of elements, inherent to the initial single-phase foil structure.

Earlier formation of chromium-rich particles was observed at decomposition of single-phase condensates of CrFeCoNiCu alloy produced by magnetron sputtering method. According to the SAED data their structure corresponds to BCC lattice with the lattice parameter of 0.294 nm [25]. Furthermore, it was shown in publications [23] that chromium-enriched particles were observed in cast CrFeCoNiCu<sub>0.5</sub> alloy. According to the data presented in the work, chromium content in these particles is 3 times higher than that of other elements. The composition of these particles is close to the Cr<sub>3</sub>FeCoNiCu<sub>0.5</sub>.

As no chromium-enriched particles were observed in the vacuum condensate structure in an as-deposited state, it was assumed that they form as a result of the decomposition of the initial FCC1-phase. Fig. 10a and Table 3 give the image of the microstructure and chemical composition of regions with different contrast formed in a single-phase vacuum condensate of CrFeCoNiCu<sub>0.7</sub> HEA, deposited at the substrate temperature of 775 K, after its annealing at the temperature of 1025 K for 2 h. However, unlike the chromium-enriched phase, observed in the cast alloys [23], this phase in vacuum condensates contains a somewhat smaller concentration of chromium, compared to Fe, Ni, Co, and Cu. It is also noteworthy that the dark-grey areas in the microstructure (enriched in chromium), as a rule, have light-colored fringes (Fig. 10a).

Proceeding from the results of previous studies of the interaction of chemical composition of different regions in microstructural images and their contrast, we can assume that at the initial stages of decomposition, chromium-enriched regions form by driving copper from the condensate initial structure to the grain boundaries. This leads to the formation of light-colored fringes around the dark-grey particles, enriched in chromium. Vacuum condensate annealing at the temperature of 1025 K for two hours does not lead to the decomposition of elements in the regions of light-grey shade, and they preserve the condensate structure in an as-deposited state.

Thus, at the intermediate stages of decomposition three structural components can be present in the foil simultaneously: two FCC phases with somewhat different lattice parameters and Cr-rich particles. The crystalline structure of the Cr-rich phase was not determined by X-ray because of low intensity of diffraction reflections of the phase, as well as their overlapping with intense peaks of FCC1 and FCC2 phases. It is worth noting that the superposition of most intense diffraction peaks will be observed for both cases of BCC [25] and FCC [23] structure of the Cr-rich phases.

In the case of a cast alloy, the particles enriched in chromium are preserved at annealing in the temperature range from 625 to 1475 K [23]. However, annealing at the temperature of 1475 K leads to a change of their chemical composition, compared to the initial one: annealing results in an increase of chromium concentration in the

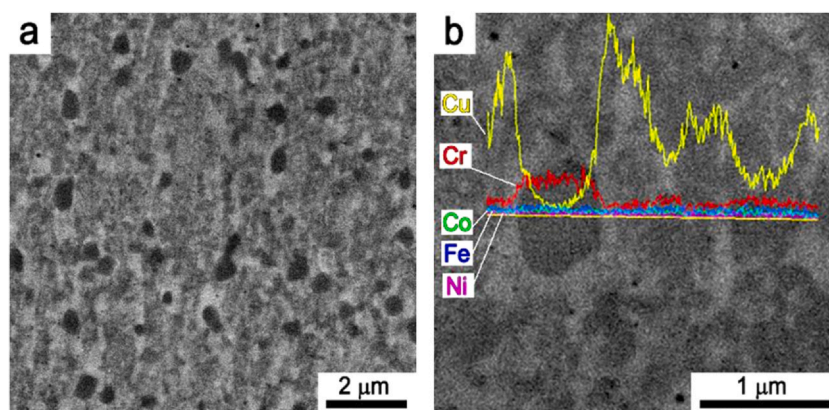


**Fig. 9.** SEM images of the cross-sectional microstructure of the CrFeCoNiCu foil deposited at substrate temperature of 775 K after annealing at the temperature of 1025 K for 2 h.

particles from 46 at% to 95 at%, whereas the content of other alloying elements decreases.

In the case of vacuum condensates of CrFeCoNiCu<sub>0.7</sub> HEA, no chromium-enriched particles were found after annealing at 1175 K for 2 h. It is supposed that such a heat treatment leads to the decomposition of the initial FCC1-phase, redistribution of elements, and, consequently, to the formation of a two-phase structure (Fig. 10b), consisting of FCC2-phase, enriched in copper (light regions) and FCC1-phase, depleted in copper with the ratio of Cr, Fe, Co, Ni and Cu elements close to the equiatomic one (regions of the grey color of different intensity).

It is noteworthy that the grains of FCC1-phase, depleted in copper, are characterized by fringed contrast, characteristic for the twin grain substructure, the formation of which was observed earlier, for instance in metals and alloys with low stacking-fault energy [35,36]. One can see that the thickness of twin domains reaches the nanosize value.

As shown by earlier conducted studies, fringed contrast of grains in electron microscopy images depends on their orientation relative to electron beam direction: at grain orientation relative to the electron beam, when some domains are in the reflecting position, they appear to be light regions in the microstructure image in BEI, while the domains in twinning orientation relative to them look like dark regions, although the chemical composition of these regions does not differ (Table 4, Fig. 10b).

Thus, annealing of foils based on CrFeCoNiCu<sub>x</sub> HEA at  $x > 0.3$ , deposited at temperatures below 925 K, leads to their decomposition with the formation of two FCC-phases, differing by their chemical composition, mainly the ratio of copper, whereas the ratio of Fe, Ni, Co and Cr elements in both the phases is approximately

**Table 3**

Chemical composition of different areas of SEM image of the CrFeCoNiCu foil (Fig. 10a).

Area number	Chemical composition, at%				
	Cr	Fe	Co	Ni	Cu
#1	35.6	19.7	20.0	14.5	10.2
#2	23.3	19.1	18.1	18.3	21.2
#3	25.2	21.1	20.1	19.4	14.2

**Table 4**

Chemical composition of different areas of SEM image of the CrFeCoNiCu foil (Fig. 10b).

Area number	Chemical composition, at%				
	Cr	Fe	Co	Ni	Cu
#1	27.4	22.8	22.4	21.4	6.0
#2	18.9	15.2	14.2	15.1	36.6
#3	26.6	22.8	22.1	21.9	6.6
#4	27.3	22.5	22.2	21.2	6.8

equiatomic. Chemical composition of FCC1 is close to CrFeNiCoCu<sub>y</sub> composition, where  $y = 0.3 \dots 0.5$ , and that of FCC2 - to CrFeNiCoCu<sub>z</sub> composition, where  $z = 2 \dots 3$ .

At the change of copper content in the condensate, the ratio of volume fractions of FCC1- and FCC2-phase is structured components changes. To illustrate this effect, Fig. 11 shows the microstructures of vacuum condensates with different content of copper after their annealing at the temperature of 1175 K. One can see that at the increase of copper content in the condensate, the volume fraction of

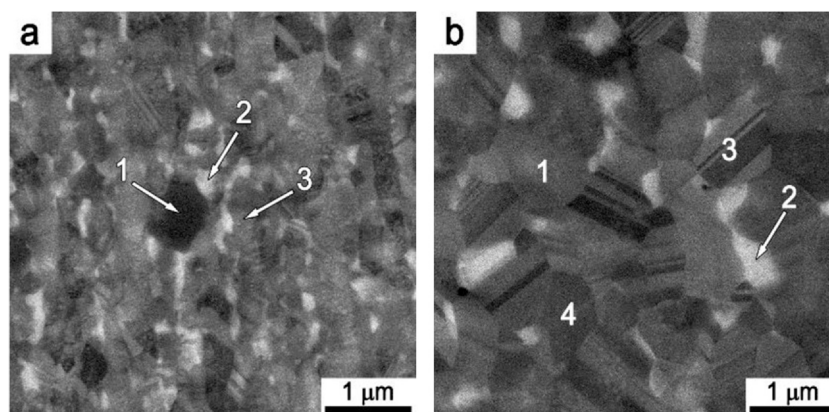


**Fig. 10.** SEM images of the cross-sectional microstructure of the CrFeCoNiCu<sub>0.7</sub> foil deposited at substrate temperature of 775 K after annealing at the temperature of 1025 K (a) and 1175 K (b) for 2 h.

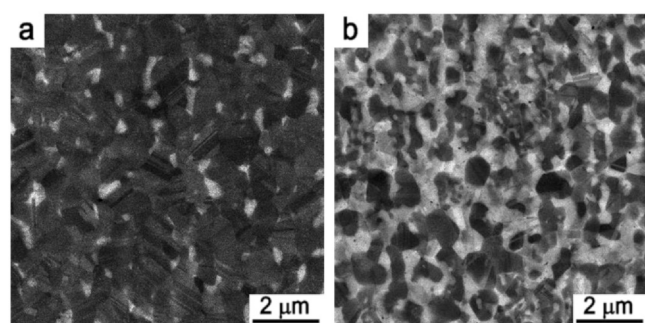


**Fig. 11.** SEM images of the cross-sectional microstructure of the CrFeCoNiCu<sub>x</sub> foil after annealing at the temperature of 1175 K for 2 h: (a)  $x = 0.7$ ; (b)  $x = 3$ .

the light-colored component of the microstructure, which is identified as FCC2-phase becomes greater, and the fraction of grains with dark contrast (FCC1-phase) becomes smaller.

It is also noteworthy that the dimensions of grains of FCC1-phase (dark component) decrease at the increase of copper content in the condensate. The reduction of the dimensions of FCC1-phase grains is here accompanied by a change of their substructure from poly-domain to single-domain one. Proceeding from the fact that precipitates of phase enriched in chromium form at the initial stage of annealing of single-phase condensates, it can be assumed that their transformation into FCC1-phase may be accompanied by the recrystallization process, which results in the formation of larger grains of FCC1-phase with poly-domain substructure. Coarsening of grains of FCC2-phase, which are located predominantly in the triple junctions of FCC1-phase grains and along their boundaries, is also observed here.

However, it is evident from Fig. 11b, an increase of volume fraction of FCC2-phase precipitates leads to the reduction of the contact area of FCC1-phase grains with each other. The absence of contact between FCC1-phase grains inhibits the recrystallization process.

Generalizing the obtained results, the process of decomposition of single-phase condensates of CrFeCoNiCu<sub>x</sub> HEAs, where  $x = 0.3...3$  during their annealing at temperatures above 925 K can be presented in the form of a scheme shown in Fig. 12.

The initial stages of decomposition of the initial solid solution structure of a multicomponent system are accompanied by the displacement of copper atoms from the regions enriched in chromium to the grain boundaries. It leads to formation of copper-rich and chromium-rich areas in the initial solid solution. Microstructural analysis leads to the assumption that the process of formation of chromium-rich particles in the case of films produced by magnetron sputtering [25] and of foils produced by EB PVD method in this work, is somewhat different. In the case of sputtered films, the particles are formed by the yield of chromium atoms from the solid solution, whereas in our case the regions enriched in chromium are formed because of the release of copper atoms from them to the periphery. As a result, in thin films Cr-rich particles often have a BCC crystalline lattice with the parameter, close to lattice parameter of pure chromium.

Furthermore, the process of the transition from a three-phase state to a two-phase state is determined by the copper content in the alloy. Irrespective of copper content, the three-phase state is unstable, and diffusion interaction of Cr-rich areas and of the initial solid solution results in formation of FCC1 phase. However, in alloys with a low copper content ( $x < 1$ ) formation of a two-phase state is accompanied by recrystallization of grains of FCC1-phase and at a larger copper content, this process is inhibited by isolation of FCC1 phase grains by those of FCC2 phase.

Coincidence of temperature ranges of decomposition of the initial solid solution of CrFeCoNiCu<sub>x</sub> HEA with running of the recrystallization processes can be regarded as an indication of the fact the stability of vacuum condensate structure below 925 K is rather the result of a low diffusion mobility of atoms, than the consequence of thermodynamic stability of a multicomponent solid solution. Apparently, for the same reason, a single-phase state forms during vapour-phase condensation at temperature below 925 K, while at a higher condensation temperature a two-phase state forms as a result of increased diffusion mobility of atoms in the solid state.

Thus, the structure of vacuum condensates of CrFeCoNiCu<sub>x</sub> HEAs, where  $x = 0.3...3$  depends both on the temperature of their deposition from the vapor phase, and of subsequent annealing of the phases. The possibility of formation of different structural states of the foil and coatings based on HEA of the same composition allows correlating their structural characteristics and mechanical properties at static (strength properties) and dynamic loading (dissipative properties) that is necessary for evaluation of practical applicability of such materials.

### 3.3. Mechanical properties of HEA foils

#### 3.3.1. Strength properties

Strength properties of foils under static loading were assessed by the indentation method. Fig. 13 shows typical diagrams describing indenter embedding at its loading and unloading for foils produced at different temperatures of deposition and subsequent treatment.

Analysis of these diagrams allowed obtaining the mechanical characteristics (Young's modulus, microhardness, and coefficient of plasticity) of the produced foils. Fig. 14a shows microhardness dependencies for the initial ingots and foils of the studied HEAs. It can be seen that the microhardness of CrFeCoNiCu foils is 1.3...2 times higher than that of the initial.

ingot, which may be a consequence of grain-boundary strengthening due to the much smaller size of the condensate grains (Hall-Patch effect). With increasing deposition temperature, the grain size of the condensate becomes larger (Fig. 4), and its microhardness approaches that of the initial ingot (Fig. 14a). From Fig. 14b one can see that Young's modulus for the two-phase CrFeCoNiCu condensate deposited at substrate temperature above 925 K, having a similar phase composition, is almost the same as for the initial ingot with the same phase composition. A slightly increased Young's modulus for the condensate deposited at a higher temperature of 1120 K may be related to the decrease in its porosity. Fig. 14c shows

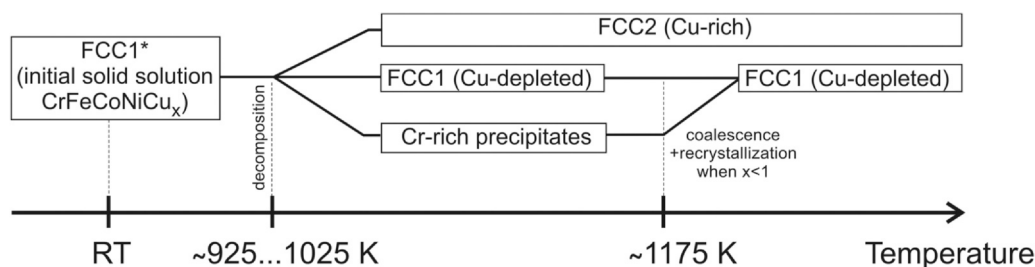


**Fig. 12.** Scheme of the phase transformation of the single-phase CrFeCoNiCu<sub>x</sub> vacuum condensates at heating.

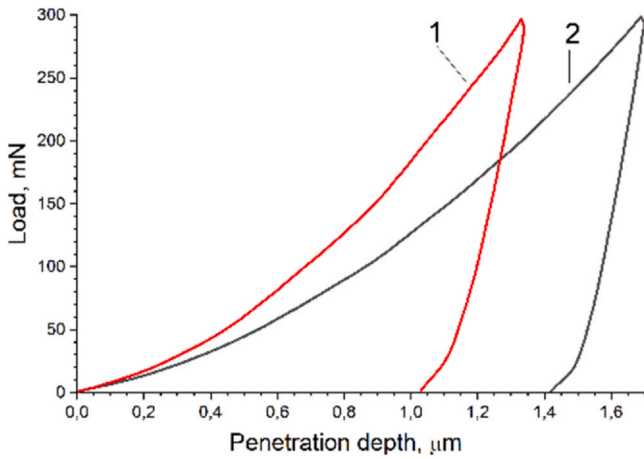


Fig. 13. The load-penetration curve for the single-phase (1) and two-phase (2) CrFeCoNiCu<sub>x</sub> condensates.

the dependencies of the coefficient of plasticity,  $\delta_{pl}$  of the ingots, and CrFeCoNiCu condensates. One can see that the coefficient of plasticity for CrFeCoNiCu condensates with nanoscale and submicron grain sizes is somewhat lower than that for the corresponding massive ingot with large grains. In this case, as deposition temperature and, correspondingly, the grain size in the condensate increase, its plasticity also increases.

### 3.3.2. Dissipative properties

Assessment of dissipative properties was conducted on samples with CrFeCoNiCu<sub>x</sub> alloy coatings in different structural states, produced by variation of their chemical composition, the temperature of deposition, and subsequent heat treatment.

Fig. 15 shows amplitude dependencies of LD  $\delta_s(<\epsilon>)$  for samples with CrFeCoNiCu<sub>x</sub> coatings in single-phase (FCC1) and two-phase (FCC1+FCC2) states. One can see that at all the deformation amplitudes and temperatures the values of the logarithmic decrement are much greater for samples with CrFeCoNiCu<sub>2</sub> and CrFeCoNiCu<sub>3</sub> coatings than for those with CrFeCoNiCu<sub>0.3</sub> coating.

Formation of a two-phase FCC1 + FCC2 structure in CrFeCoNiCu<sub>3</sub> coating annealed at the temperature of 1025 K causes some decrease of its DC level at room temperature. Yet, the DC of the samples with two-phase coatings at elevated temperatures increases by the factor of 1.5 as compared to a sample with a single-phase coating (Fig. 15b). It is worth noting that LD values observed during the coating heating and cooling show good reproducibility.

One can also see (Fig. 15) that at temperature increase from 295 K to 720 K the DC level increases significantly more for a sample with a two-phase coating than for a sample with a single-phase coating. It is known [37], that formation of a heterophase structure in the alloys is usually accompanied by increase of the material DC level as a result of formation of a “softer phase” in the “hard” matrix, appearance of defects of grain boundary structure, formation of special boundaries between different phases, etc. Experimental results, obtained in this work, do not allow unambiguously establishing the nature of this phenomenon in CrFeCoNiCu HEA. However, note the fact that increase of copper content in the coating, enhances the impact of temperature on DC level of the samples.

It suggests that the level of dissipation of mechanical energy in the samples is associated with copper distribution in the coating grains: single-phase structure of the coating is characterized by uniform distribution of copper in the initial solid solution, while at its decomposition copper segregates to the grain boundaries. As a result, copper-rich FCC2 phase forms an interphase with FCC1 phase, depleted in copper. Therefore, in can be anticipated that the

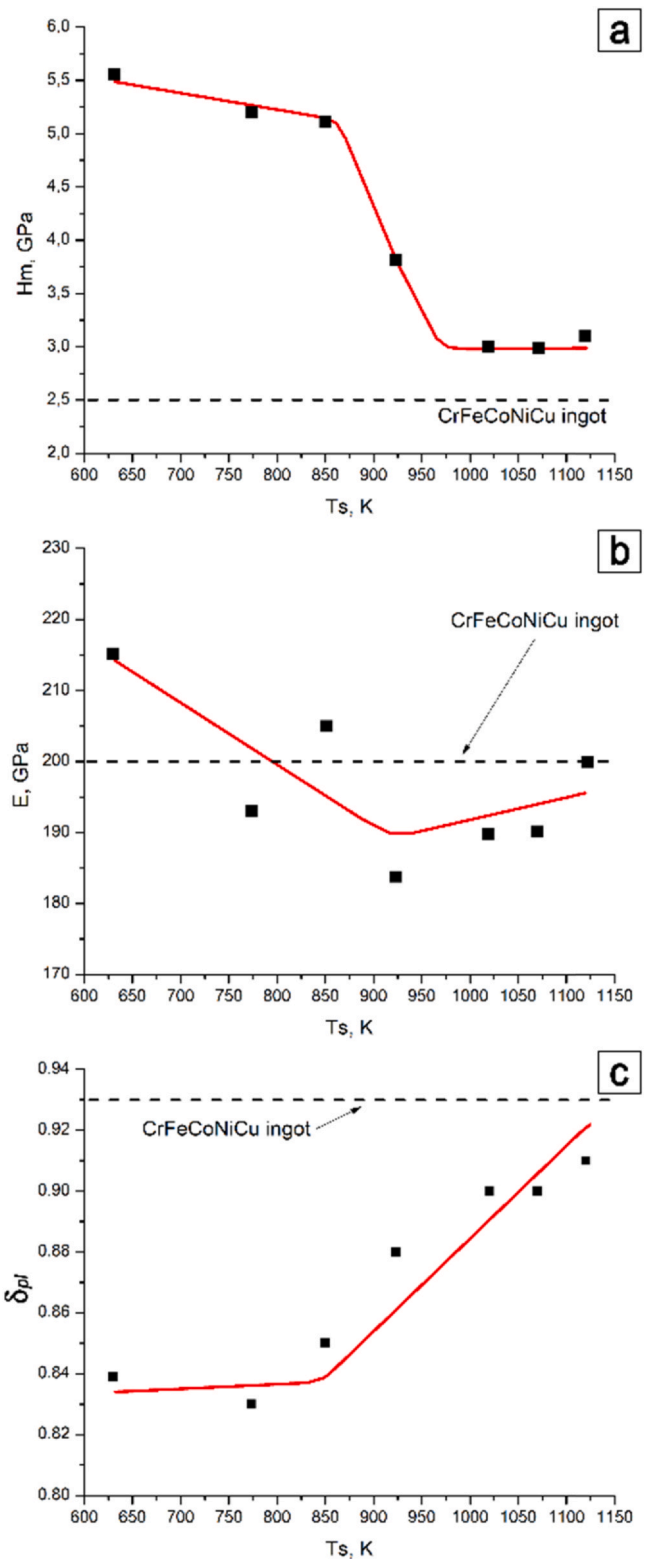
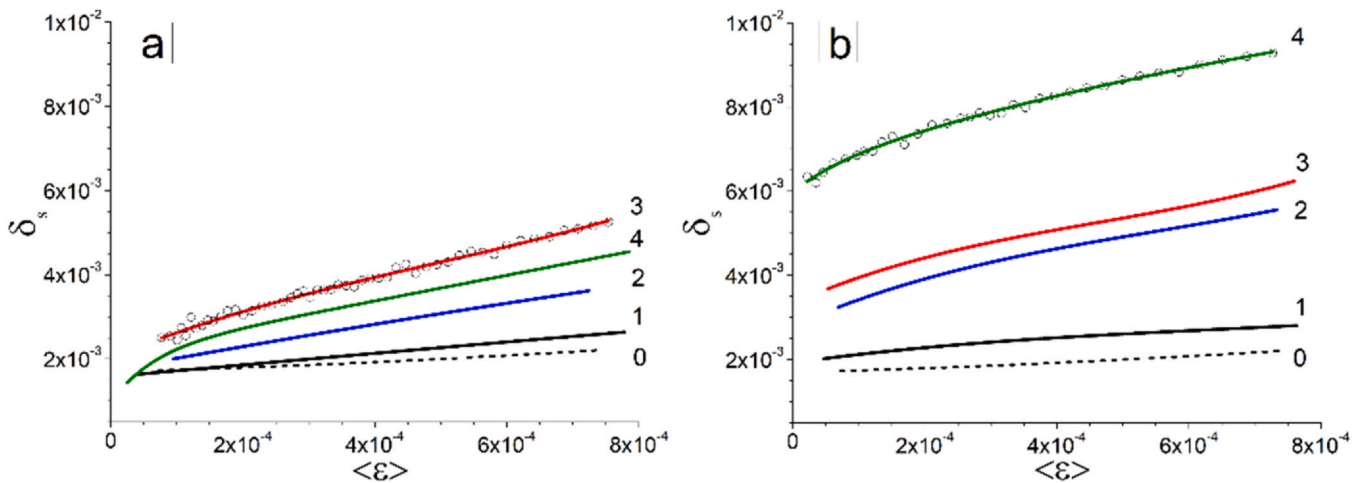


Fig. 14. Dependence of microhardness (a), Young's modulus (b), and plasticity coefficient (c) on substrate temperature for CrFeCoNiCu condensates deposited at different substrate temperatures.

processes of grain-boundary diffusion of copper atoms at alternating elastic stresses can be activated in the decomposed alloy at temperature rise.

More over, we cannot exclude the fact that the isostructural decomposition of the initial solid solution leads to the formation of



**Fig. 15.** Amplitude dependencies of LD of samples with coatings in single-phase state (FCC1 structure) with CrFeCoNiCu0.3 (curve 1), CrFeCoNiCu2 (curve 2), CrFeCoNiCu3 (curve 3) compositions and of two-phase CrFeCoNiCu3 coatings (FCC1 +FCC2 structure) (curve 4) at temperatures of 295 K (a) and 720 K (b), respectively. Curve 0 shows amplitude dependencies of LD for uncoated substrates.

special boundaries of coherent conjugation of FCC lattices with different crystallographic parameters.

In such materials, the hysteresis motion of interphases can occur at cyclic deformation and, hence, additional scattering of mechanical energy. The joint action of the above mechanisms of energy scattering accounts for the higher level of DC of vacuum condensates with a two-phase FCC1 +FCC2 structure, in the studied range of temperatures and deformation amplitudes.

It is clear that in order to establish the contribution of these mechanisms of dissipation of elastic energy oscillations into ensuring a high level of energy dissipation in CrFeCoNiCu HEA with a high copper content, additional studies are required, aimed at clarifying the interrelation of microstructural characteristics of the alloys and their DC level.

Fig. 16 gives amplitude dependencies of eigenvalues of loss factor  $\eta(\epsilon)$  for the material of CrFeCoNiCu<sub>3</sub> coating with a two-phase FCC1 +FCC2 structure. One can see that in the studied temperature range they are described by monotonic moderately increasing amplitude dependencies of  $\eta(\epsilon)$ , for which the values of the loss factor at temperatures of 470...670 K are equal to 0.02...0.045.

This is commensurate with DC level of such highly damping materials as magnesium alloys AZ31B-F ( $\eta = 0.016$ ), MIF-cast alloy ( $\eta = 0.04$ ), or NIVCO-10 alloy ( $\eta = 0.016$ ) [38].

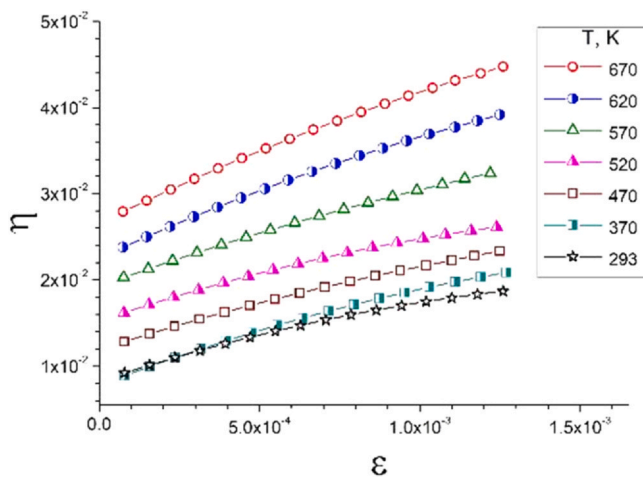


**Fig. 16.** Amplitude dependencies on eigenvalues of loss factor  $\eta(\epsilon)$  for the material of CrFeCoNiCu<sub>3</sub> coating with a two-phase FCC1 +FCC2 structure at different ambient temperature.

It follows from the presented results that HEA-based vacuum condensates, both in single-phase and in the two-phase state have a high level of damping capacity, which rises with temperature. Such dissipative properties of vacuum condensates based on the CrFeCoNiCu<sub>x</sub> system open up new capabilities for their application as damping coatings or fabrication of structural elements operating under vibration conditions.

#### 4. Conclusions

1. By the example of condensates of CrFeCoNiCu<sub>x</sub> alloys produced by EB PVD, the influence of both the copper content, x in the range of 0...3 and deposition temperature in the range of 525...1275 K on their phase composition and microstructure has been studied.
2. Condensates of CrFeCoNiCu<sub>x</sub> alloy with  $x < 0.3$ , irrespective of deposition temperature, have a single-phase FCC structure, the chemical composition of which corresponds to that of the ingot. At  $x > 0.3$  the phase composition of the condensate depends on deposition temperature: a single-phase FCC structure of the condensate forms at deposition temperature below 925 K, while a two-phase structure consisting of FCC-phases enriched and depleted in copper forms at temperatures above 925 K.
3. Annealing of single-phase condensates of CrFeCoNiCu<sub>x</sub> HEA at  $x > 0.3$  results in the decomposition of single-phase FCC structure into two FCC structures, similar to FCC structures formed during deposition of these alloys at temperatures above 925 K. The transition of the single-phase structural state of vacuum condensate into a two-phase one during annealing is accompanied by the formation of an intermediate phase rich in chromium, which dissolves as a result of diffusion interaction with FCC phases, differing by their copper content.
4. It is shown that CrFeCoNiCu foils in the single-phase state are characterized by increased microhardness level, as compared to the cast alloy. However, the coefficient of plasticity remains low. A transition into the two-phase state results in the microhardness decrease, although it remains higher than that in the cast ingot. The plasticity coefficient of the condensate becomes higher and tends to the level of the cast state of the alloy.
5. The damping capacity of coatings based on CrFeCoNiCu<sub>x</sub> alloy depends both on its copper content and phase composition. It is shown that the transition from the single-phase state of the alloy into the three-phase or two-phase one leads to the damping capacity increase. The increase of damping capacity of the

coating is the greater, the higher the copper content in the coating. It is found that coatings with eigenvalues of the loss factor on the level of those of highly-damping materials can be obtained on the base of CrFeCoNiCu<sub>x</sub> alloy, where  $x = 2.5...3$

### CRedit authorship contribution statement

**A.I. Ustinov:** Conceptualization, Methodology, Supervision. **S.A. Demchenkov:** Investigation, Visualization, Writing – original draft. **T.V. Melnychenko:** Investigation. **V.S. Skorodzievskii:** Investigation, Formal analysis, Writing – reviewing & editing. **S.S. Polishchuk:** Investigation, Visualization, Writing – reviewing & editing.

### Declaration of Competing Interest

The authors declare that they have no known competing financial interests or personal relationships that could have appeared to influence the work reported in this paper.

### References

- [1] B.S. Murty, J.W. Yeh, S. Ranganathan, Chapter 2 - High-Entropy Alloys: Basic Concepts, in: B.S. Murty, J.W. Yeh, S. Ranganathan (Eds.), *High Entropy Alloys*, Butterworth-Heinemann, 2014, pp. 13–35, <https://doi.org/10.1016/B978-0-12-800251-3.00002-X>
- [2] C.J. Tong, M.R. Chen, S.K. Chen, J.W. Yeh, T.T. Shun, S.J. Lin, S.Y. Chang, Mechanical performance of the Al<sub>x</sub>CoCrCuFeNi high-entropy alloy system with multi-principal elements, *Metall. Mater. Trans. A* 36 (2005) 1263–1271, <https://doi.org/10.1007/s11661-005-0218-9>
- [3] M. Wang, H. Cui, Y. Zhao, C. Wang, N. Wei, X. Gao, Q. Song, Enhanced strength and ductility in a spark plasma sintered CoCrCu<sub>0.5</sub>NiAl<sub>0.5</sub> high-entropy alloy via a double-step ball milling approach for processing powders, *Mater. Sci. Eng. A* 762 (2019) 138071, <https://doi.org/10.1016/j.msea.2019.138071>
- [4] C.Y. Hsu, C.C. Juan, W.R. Wang, T.S. Sheu, J.W. Yeh, S.K. Chen, On the superior hot hardness and softening resistance of AlCoCr(x)FeMo(0.5)Ni high-entropy alloys, *Mat. Sci. Eng. A-Struct.* 528 (2011) 3581–3588, <https://doi.org/10.1016/j.msea.2011.01.072>
- [5] M.H. Chuang, M.H. Tsai, W.R. Wang, S.J. Lin, J.W. Yeh, Microstructure and wear behavior of Al<sub>x</sub>Co<sub>1.5</sub>CrFeNi<sub>1.5</sub>Ti<sub>y</sub> high-entropy alloys, *Acta Mater.* 59 (2011) 6308–6317, <https://doi.org/10.1016/j.actamat.2011.06.041>
- [6] V. Dolique, A.-L. Thomann, P. Brault, Y. Tessier, P. Gillon, Thermal stability of AlCoCrCuFeNi high entropy alloy thin films studied by in-situ XRD analysis, *Surf. Coat. Tech.* 204 (2010) 1989–1992, <https://doi.org/10.1016/j.surfcoat.2009.12.006>
- [7] Z. Wu, S.A. David, Z. Feng, H. Bei, Weldability of a high entropy CrMnFeCoNi alloy, *Scr. Mater.* 124 (2016) 81–85, <https://doi.org/10.1016/j.scriptamat.2016.06.046>
- [8] Y. Lu, H. Huang, X. Gao, C. Ren, J. Gao, H. Zhang, Sh Zheng, Q. Jin, Y. Zhao, Ch Lu, T. Wang, T. Li, A promising new class of irradiation tolerant materials: Ti<sub>2</sub>ZrHfV<sub>0.5</sub>Mo<sub>0.2</sub> high-entropy alloy, *J. Mater. Sci. Technol.* 35 (3) (2019) 369–373, <https://doi.org/10.1016/j.jmst.2018.09.034>
- [9] S.G. Ma, P.K. Liaw, M.C. Gao, J.W. Qiao, Z.H. Wang, Y. Zhang, Damping behavior of Al<sub>x</sub>CoCrFeNi high-entropy alloys by a dynamic mechanical analyzer, *J. Alloy. Compd.* 604 (2014) 331–339, <https://doi.org/10.1016/j.jallcom.2014.03.050>
- [10] I.O. Husarova, O.M. Potapov, T.A. Manko, Y.V. Falchenko, L.V. Petrushintsev, G.A. Frolov, V.P. Soltsev, Problems of creations of reusable spacecraft heat protection, *Technol. Syst.* 81 (4) (2017) 47–55, <https://doi.org/10.29010/081.6>
- [11] B.R. Braeckman, F. Boydens, H. Hidalgo, P. Dutheil, M. Jullien, A.-L. Thomann, D. Depla, High entropy alloy thin films deposited by magnetron sputtering of powder targets, *Thin Solid Films* 580 (2015) 71–76, <https://doi.org/10.1016/j.tsf.2015.02.070>
- [12] L.R. Shaginyan, V.F. Gorban', N.A. Krapivka, S.A. Firstov, I.F. Kopylov, Properties of coatings of the Al–Cr–Fe–Co–Ni–Cu–V high entropy alloy produced by the magnetron sputtering, *J. Superhard Mater.* 38 (2016) 25–33, <https://doi.org/10.3103/S1063457616010044>
- [13] X. Li, Z. Zheng, D. Dou, J. Li, Microstructure and properties of coating of FeAl<sub>2</sub>CrCoMn high entropy alloy deposited by direct current magnetron sputtering, *Mat. Res.* 19 (4) (2016) 802–806, <https://doi.org/10.1590/1980-5373-MR-2015-0536>
- [14] A. Stefaniak, The kinetics of growth of high entropy alloy layers sputtered on Tungsten powder substrate, *World Sci. N.* 76 (2017) 60–65.
- [15] S.Y. Chang, S.Y. Lin, Y.C. Huang, Microstructures and mechanical properties of multi-component (AlCrTaTiZr)<sub>Nx</sub>Cy nanocomposite coatings, *Thin Solid Films* 519 (2011) 4865–4869, <https://doi.org/10.1016/j.tsf.2011.01.043>
- [16] O.V. Sobol', A.A. Andreev, V.F. Gorban', N.A. Krapivka, V.A. Stolbovoi, I.V. Serdyuk, V.E. Fil'chikov, Reproducibility of the single-phase structural state of the multielement high-entropy Ti–V–Zr–Nb–Hf system and related superhard nitrides formed by the vacuum-arc method, *Tech. Phys. Lett.* + 38 (7) (2012) 616–619, <https://doi.org/10.1134/S1063785012070127>
- [17] L.M. Wang, C.C. Chen, J.W. Yeh, S.T. Ke, The microstructure and strengthening mechanism of thermal spray coating Ni<sub>x</sub>Co<sub>0.6</sub>Fe<sub>0.2</sub>Cr<sub>y</sub>Si<sub>z</sub>AlTi<sub>0.2</sub> high-entropy alloys, *Mater. Chem. Phys.* 126 (2011) 880–885, <https://doi.org/10.1016/j.matchemphys.2010.12.022>
- [18] P.K. Huang, K.-W. Yeh, T.T. Shun, S.-K. Chen, Multi-principal-element alloys with improved oxidation and wear resistance for thermal spray coating, *Adv. Eng. Mater.* 6 (2004) 74–78, <https://doi.org/10.1002/adem.200300507>
- [19] A.I. Ustinov, S.S. Polishchuk, S.A. Demchenkov, T.V. Melnychenko, V.S. Skorodzievskii, Formation of thin foils of high-entropy CrFeCoNiCu alloys by EB-PVD process, *Surf. Coat. Technol.* 403 (2020) 126440, <https://doi.org/10.1016/j.surfcoat.2020.126440>
- [20] X. Xian, L. Lin, Z. Zhong, C. Zhang, C. Chen, K. Song, J. Cheng, Y. Wu, Precipitation and its strengthening of Cu-rich phase in CrMnFeCoNiCu<sub>x</sub> high entropy alloys, *Mater. Sci. Eng. A-Struct.* 713 (2018) 134–140, <https://doi.org/10.1016/j.msea.2017.12.060>
- [21] T. Nagase, Microstructure of Co–Cr–Fe–Mn–Ni–Cu and Co–Cr–Fe–Mn–Ni–Ag high entropy alloys with liquid phase separation, *Mater. Sci. Forum* 941 (2018) 1238–1241, <https://doi.org/10.4028/www.scientific.net/MSF.941.1238>
- [22] Y. Zhang, Zh Chen, D. Cao, J. Zhang, P. Zhang, Q. Tao, X. Yang, Concurrence of spinodal decomposition and nano-phase precipitation in a multi-component AlCoCrCuFeNi high-entropy alloy, *J. Mater. Res. Technol.* 8 (1) (2019) 726–736, <https://doi.org/10.1016/j.jmrt.2018.04.020>
- [23] C.-M. Lin, H.-L. Tsai, Equilibrium phase of high-entropy FeCoNiCrCu<sub>0.5</sub> alloy at elevated temperature, *J. Alloy. Compd.* 489 (1) (2010) 30–35, <https://doi.org/10.1016/j.jallcom.2009.09.041>
- [24] A. Fourmont, A.S. Rogachev, S. Le Gallet, O. Politano, D. Yu. Kovalev, N.A. Kochetov, N.F. Shkodich, S.G. Vadchenko, F. Baras, Thermal Stability of Medium- and High-Entropy Alloys of 3d-Transition Metals, *J. Phase Equilib. Diffus.* 2021, <https://doi.org/10.1007/s11669-021-00903-y>
- [25] M. Arfaoui, G. Radnóczy, V. Kovács Kis, Transformations in CrFeCoNiCu high entropy alloy thin films during in-situ annealing in TEM, *Coatings* 10 (1) (2020) 60, <https://doi.org/10.3390/coatings10010060>
- [26] N. Park, I. Watanabe, D. Terada, Y. Yokoyama, P.K. Liaw, N. Tsuji, Recrystallization behavior of CoCrCuFeNi high-entropy alloy, *Metall. Mater. Trans. A* 46 (2015) 1481–1487, <https://doi.org/10.1007/s11661-014-2594-5>
- [27] A.I. Ustinov, V.S. Skorodzievskii, S.A. Demchenkov, S.S. Polishchuk, T.V. Melnichenko, Effect of the structure of vacuum condensates of high entropy alloys of Cr–Fe–Co–Ni–Cu system on their mechanical properties, *Electrometall. Today* 4 (2020) 16–22, <https://doi.org/10.37434/sem2020.04.03>
- [28] S.R. Ignatovich, I.M. Zakiev, D.I. Borisov, Material surface layer damage estimation for cyclic loading conditions using the nanoindenting and nanoscratching techniques, *Strength Mater.* + 38 (2006) 428–434, <https://doi.org/10.1007/s11223-006-0061-2>
- [29] Yu.V. Milman, Plasticity characteristic obtained by indentation, *J. Phys. D: Appl. Phys.* 41 (2008) 074013, <https://doi.org/10.1088/0022-3727/41/7/074013>
- [30] A.I. Ustinov, A.A. Nekrasov, V.A. Perederiy, A.M. Sviridov, V.S. Skorodzievskii, V.N. Taranenko, Device for dissipate properties research of metallic flat samples with coating, *Zavod. Lab.* 10 (2012) 41–44 (in Russian).
- [31] A. Ustinov, S. Polishchuk, V. Skorodzievskii, V. Bliznuk, Effect of grain size on damping capacity of quasicrystalline Al–Cu–Fe materials, *Surf. Coat. Tech.* 202 (2008) 5812–5816, <https://doi.org/10.1016/j.surfcoat.2008.05.049>
- [32] A.I. Ustinov, V.S. Skorodzievskii, N.S. Kosenko, A study of the dissipative properties of homogenous materials deposited as coatings. Part 1: method for the determination of the amplitude dependence of the true vibration decrement for the coating material, *Strength Mater.* + 39 (6) (2007) 663–670, <https://doi.org/10.1007/s11223-007-0076-3>
- [33] A. Rivière, Measurement of high damping: techniques and analysis, *J. Alloy. Compd.* 355 (1–2) (2003) 201–206, [https://doi.org/10.1016/S0925-8388\(03\)00287-1](https://doi.org/10.1016/S0925-8388(03)00287-1)
- [34] Y. Zhang, Zh Chen, D. Cao, J. Zhang, P. Zhang, Q. Tao, X. Yang, Concurrence of spinodal decomposition and nano-phase precipitation in a multi-component AlCoCrCuFeNi high-entropy alloy, *J. Mater. Res. Technol.* 8 (1) (2019) 726–736, <https://doi.org/10.1016/j.jmrt.2018.04.020>
- [35] A.I. Ustinov, V.S. Skorodzievskii, O.V. Fesiu, Damping capacity of nanotwinned copper, *Acta Mater.* 56 (15) (2008) 3770–3776, <https://doi.org/10.1016/j.actamat.2008.04.009>
- [36] A.I. Ustinov, O.V. Fesiu, Effect of substrate temperature on the structure of Ag–Cd condensates, *Surf. Coat. Tech.* 204 (11) (2010) 1774–1778, <https://doi.org/10.1016/j.surfcoat.2009.11.014>
- [37] H. Lu, X. Wang, T. Zhang, Z. Cheng, Q. Fang, Design, fabrication, and properties of high damping metal matrix composites – a review, *Materials* 2 (3) (2009) 958–977, <https://doi.org/10.3390/ma2030958>
- [38] J. Zhang, R.J. Perez, E.J. Lavernia, Documentation of damping capacity of metallic, ceramic and metal-matrix materials, *J. Mat. Sci.* 28 (1993) 2395–2404, <https://doi.org/10.1007/BF01151671>